

Cobalt anchored CN sheet boosts the performance of electrochemical CO oxidation

Xu Liu(刘旭), Jun-Chao Huang(黄俊超), and Xiang-Mei Duan(段香梅)
Citation: Chin. Phys. B, 2021, 30 (**6**): 067104. DOI: 10.1088/1674-1056/abfbd7
Journal homepage: http://cpb.iphy.ac.cn; http://iopscience.iop.org/cpb

What follows is a list of articles you may be interested in

Investigation of electronic, elastic, and optical properties of topological electride Ca_3Pb via first-principles calculations

Chang Sun(孙畅), Xin-Yu Cao(曹新宇), Xi-Hui Wang(王西惠), Xiao-Le Qiu(邱潇乐), Zheng-Hui Fang(方铮辉), Yu-Jie Yuan(袁宇杰), Kai Liu(刘凯), and Xiao Zhang(张晓)
Chin. Phys. B, 2021, 30 (**5**): 057104. DOI: 10.1088/1674-1056/abec38

First-principles calculations of K-shell x-ray absorption spectra for warm dense ammonia

Zi Li(李孜), Wei-Jie Li(李伟节), Cong Wang(王聪), Dafang Li(李大芳), Wei Kang(康炜), Xian-Tu He(贺贤土), and Ping Zhang(张平)
Chin. Phys. B, 2021, 30 (**5**): 057102. DOI: 10.1088/1674-1056/abdb1b

First-principles investigation of the valley and electrical properties of carbon-doped α-graphyne-like BN sheet

Bo Chen(陈波), Xiang-Qian Li(李向前), Lin Xue(薛林), Yan Han(韩燕), Zhi Yang(杨致), and Long-Long Zhang(张龙龙)
Chin. Phys. B, 2021, 30 (**5**): 057101. DOI: 10.1088/1674-1056/abddac

Ultra-low Young's modulus and high super-exchange interactions in monolayer CrN: A promising candidate for flexible spintronic applications

Yang Song(宋洋), Yan-Fang Zhang(张艳芳), Jinbo Pan(潘金波), and Shixuan Du(杜世萱)
Chin. Phys. B, 2021, 30 (**4**): 047105. DOI: 10.1088/1674-1056/abdb20

First-principles calculations of F-, Cl-, and N-related defects of amorphous SiO_2 and their impacts on carrier trapping and proton release

Xin Gao(高鑫), Yunliang Yue(乐云亮), Yang Liu(刘杨), and Xu Zuo(左旭)
Chin. Phys. B, 2021, 30 (**4**): 047104. DOI: 10.1088/1674-1056/abe3f7

Cobalt anchored CN sheet boosts the performance of electrochemical CO oxidation*

Xu Liu(刘旭), Jun-Chao Huang(黄俊超), and Xiang-Mei Duan(段香梅)†

School of Physical Science and Technology, Ningbo University, Ningbo 315211, *China*

(Received 15 March 2021; revised manuscript received 21 April 2021; accepted manuscript online 27 April 2021)

Single-atom catalysts (SACs) have attracted great interest due to their significant roles played in applications of environmental protection, energy conversion, energy storage, and so on. Using first-principles calculations with dispersion-correction, we investigated the structural stability and catalytic activity of Co implanted CN sheet towards CO oxidation. The adsorption energy of CO and O_2 on the catalysts Co@CN and 2Co@CN are close, thus preventing CO poisoning. Among three possible CO oxidation mechanisms, termolecular Eley-Rideal is the most appropriate reaction path, and the corresponding rate-limiting reaction barriers of the two systems are 0.42 eV and 0.38 eV, respectively.

Keywords: first-principles calculations, single-atom catalyst, CO oxidation, rate-limiting reaction barrier

PACS: 71.15.Mb, 68.43.Bc, 34.50.Lf, 34.70.+e **DOI:** 10.1088/1674-1056/abfbd7

1. Introduction

As greenhouse gases like CO get increased,[1] researchers are trying their best to find solutions to decrease the content of CO in the air.[2] One of the most promising methods is to convert CO to CO_2 by a highly effective catalyst.[3,4] So far, considerable efforts have been made to develop novel and efficient catalysts for CO oxidation. Some typical noble metals can effectively catalyze CO oxidation, such as Pt,[5] Pd,[6] Ru,[7] and Au.[8] However, considering the low cost, environmental friendliness, and outstanding thermal stability, researchers start to develop noble-free metals gradually and achieve certain success in CO oxidation.[9] Adhering to further increase the catalytic performance and reduce the cost, the view of researchers turns to single-atom catalysts (SACs)[10] for their high site density, high specify, and low cost.[11]

Two-dimensional (2D) materials are extensively applied in various catalytic reactions as substrates owing to their large surface area, high thermal stability, and easily manufacture, such as graphene,[12,13] MoS,[14,15] hexagonal boron nitride monolayers (h-BN),[16,17] and graphic carbon nitride (CN,[18–20] C_2N,[21,22] and C_3N_4[23–25]). Many 2D materials are rich in electron pairs to combine with metal ions, and it seems easy to recognize active sites. Besides, due to the crude or artificial vacancies, 2D materials can be used as prominent supports to host metal atoms and get high stable catalyst. In the experiment, SACs can be synthesized using the mass-selected soft-landing technique, improved wet chemistry methods, or atomic layer deposition methods. Many studies showed that defects of the support materials could serve as anchoring sites for metal clusters and even single atom.[26]

It is reported that carbon nitride (CN), successfully synthesized in the experiment, can be applied in He separation,[25] H_2 storage,[27] water decomposition,[28,29] and CO oxidation.[20] Co atom, as an ideal noble-free metal, has a good performance in CO oxidation, even surpassing traditional noble metal catalysts. For instance, experimental works showed that the Co atom in Co_3O_4 shows strong catalytic activity in CO oxidation at low temperature.[30,31] However, the reaction barrier of Co-anchored graphene (Co@Gra) is as high as 0.65 eV,[32] which cannot be carried out at room temperature. In order to improve the performance, researchers start to introduce defects in graphene-based SAC, and the reaction barrier of Co@Sv-Gra is decreased by 0.23 eV.[32] Co implanted h-BN and g-C_3N_4 are also reported as excellent catalysts for CO oxidation, and the reaction barriers of Co@h-BN[33] and Co@g-C_3N_4[34] are 0.41 eV and 0.21 eV, respectively. The catalytic behavior of Co-anchored CN in the CO oxidation reaction is worth studying.

Based on first-principles calculations, we investigated CO oxidation on Co anchored planar CN sheet. Our results show that the Co atom(s) can perfectly bind to the CN monolayer and maintain the stability of the whole system. When O_2 and CO molecules are adsorbed over Co/2Co@CN, the gas molecules are activated through electron "acceptance donation" interaction between gas molecules and the transition metal. Furthermore, Co anchored CN systems possess superior catalytic activity toward the CO oxidation reaction.

2. Computation details

The calculations are performed based on density functional theory (DFT) by the Vienna *ab initio* simulation pack-

*Project supported by the National Natural Science Foundation of China (Grant Nos. 11574167 and 11874033).

†Corresponding author. E-mail: duanxiangmei@nbu.edu.cn

© 2021 Chinese Physical Society and IOP Publishing Ltd

age (VASP).[35] The Perdew–Burke–Ernzerh (PBE) functional of generalized gradient approximation (GGA) with the semi-empirical van der Waals (vdW) method of Grimme (DFT-D2) was used to handle the exchange and correlation functionals.[36,37] The cutoff energy is set to be 500 eV. The convergence tolerance for the geometry optimization is 10^{-4} eV for the energy and 10^{-2} eV/Å for the force. A vacuum space of 20 Å is adopted to avoid interaction between two adjacent images. The reciprocal space is sampled with a $3 \times 3 \times 1$ k-point grid generated automatically using the Monkhorst-Pack method[38] for optimization. A Hubbard U term was added to the PBE functional (DFT+U) to describe partially filled d orbitals. The on-site Coulomb interaction (U) of 4 eV and exchange interaction (J) of 1 eV were applied.[39] Additionally, we used the climbing image nudged elastic band (CI-NEB) method[40] to search for transition states to investigate the reaction paths. Bader charge analysis is adopted to obtain the number of transferred electrons.[41] The first principles molecular dynamics (MD) simulations at 300 K with a time step of 1 fs are performed to check the structural stability.

Taking Co@CN as an example, the binding energy (E_b) of Co on CN is defined as the energy difference between the Co atomically deposited CN and the separated CN plus the freestanding Co atom, that is $E_b = E_{Co@CN} - E_{CN} - E_{Co}$. The more negative binding energy, the more energy advantage the anchoring of Co on the substrate.

The adsorption energy (E_a) of the gas molecules is obtained by the energy difference between the absorbed Co@CN and the gaseous species plus the bare Co@CN. E_a can be expressed as $E_a = E_{adsorbate+Co@CN} - E_{adsorbate} - E_{Co@CN}$. The charge density difference $\Delta\rho$ is used to describe the electronic interaction between the substrate and the adsorbate, $\Delta\rho = \rho_{adsorbate/support} - \rho_{adsorbate} - \rho_{support}$. Here $\rho_{adsorbate/support}$, $\rho_{adsorbate}$, and $\rho_{support}$ are the corresponding charge densities of the combined system, the free adsorbate, and the bare support, respectively.

3. Results and discussion

3.1. One and two Co atoms anchored CNs

The calculated lattice constant of CN is 7.13 Å, the C–N and C–C bond lengths are 1.35 Å and 1.52 Å, respectively. The results are in good agreement with the reported values of 7.12 Å, 1.34 Å, and 1.54 Å.[27,28] A $2 \times 2 \times 1$ supercell containing 24 carbon and 24 nitrogen atoms was established. The intrinsic hole surrounded by six sp^2 bonded nitrogen atoms is beneficial for Co atom anchoring. We consider three possible sites for Co landing on CN, find the most favorable configuration is the one shown in Fig. 1(a), where the Co atom bonds to two edge N atoms with a bond length of 1.85 Å and keeps its planar geometric structure undistorted (see Fig. 1(c)). The most stable geometry for two Co atoms on CN is shown in Fig. S1(a), with the Co–N bond length of 1.81 Å and the Co–Co distance of 2.39 Å. The corresponding binding energy is calculated to be −3.77 eV and −3.26 eV/atom for Co@CN and 2Co@CN, respectively, indicating the strong interaction between the Co atom and CN monolayer. For comparison, the data are listed in Table 1, where the cohesive energies per atom of the bulk metals E_c (−4.39 eV) are taken from experiments.[42]

Table 1. The binding energies (eV) for Co, Bader charge Q ($|e|$) from Co to the substrate, the bond length of Co−N (Å), magnetic moment (μ_B), and the ratio of E_b/E_c for the most favorable Co adsorptions on CN.

Metal	E_b	Co–N distance	Q	Magnetic moment	E_b/E_c
Co	−3.77	1.85	0.72	2.68	0.86
2Co	−3.26	1.81	1.19	4.00	0.74

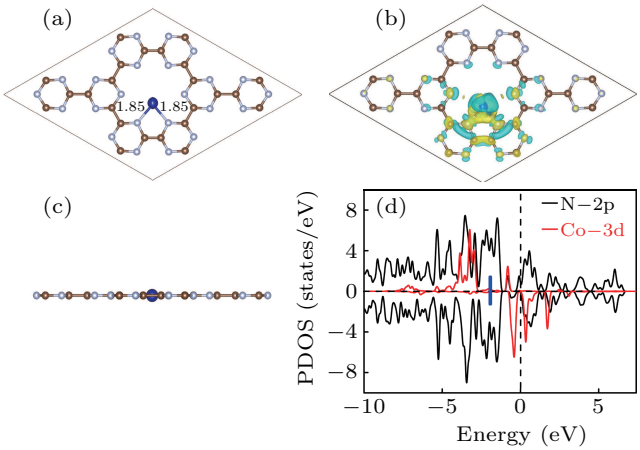


Fig. 1. The top (a) and side view (c) of optimized atomic configuration, the charge density difference plots (b) with an iso-surface value of $0.003|e|$/Bohr^3, as well as spin-polarized PDOS (d) for Co@CN. The charge accumulation and depletion regions are represented in yellow and blue, respectively. The bold blue short line points to the d-band center (−1.77 eV) of Co atom.

The transition metals have a tendency of forming clusters, then we investigate the stability of Co@CN by CI–NEB and MD methods. As shown in Figs. 2(a) and 2(b), the diffusion barrier for Co from one stable site to another in the neighboring hole is 2.62 eV. Such a large diffusion barrier conforms that the single Co atom binds with the CN monolayer steadily and hard to move. On the other hand, the large E_b/E_c ratios of 0.86 and 0.74 for single and double cobalt on the substrate manifest that Co atoms prefer a 2D growth morphology on CN. Furthermore, MD results manifest that the structure remains undistorted at room temperature (see Figs. 2(d) and 2(e)). Charge transfers from Co and 2Co to CN monolayer are $0.72|e|$ and $1.19|e|$, respectively. Comparing the energy band structure of pure CN monolayer with that of Co@CN and 2Co@CN in Fig. S2, the bands dominated by N-2p orbitals in Co@CN and 2Co@CN show that there is a semiconductor to metal transition.

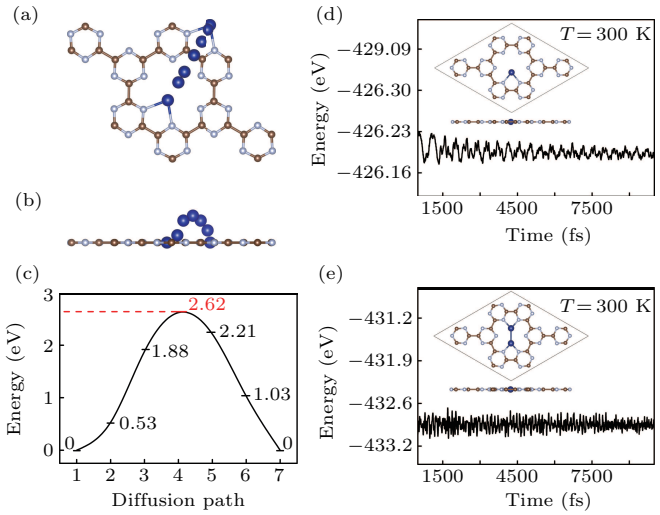


Fig. 2. The top (a) and side view (b) of diffusion path diagram and relative energy (c). The results of molecular dynamics (MD) simulations (d) and (e).

As shown in Fig. 1(b) and Fig. S1(b), the charge rearrangement mainly occurs among the Co atom(s) and the twoedged N atoms. To better understand its physical mechanism, partial density of states (PDOS) is plotted in Fig. 1(d) and Fig. S1(d). The overlapped peaks caused by orbital hybridization appearing between Co-3d and N-2p states illustrate that the single Co atom(s) can be viewed as an active site. The insertion of the second Co atom proves the ability of catalytic because the d-band center deviates from the Fermi level.[43] The magnetic momentum for Co and 2Co@CN is 2.68 μ_B and 4.0 μ_B, respectively.

3.2. Adsorption of species involved in the CO oxidation

The thermodynamics of a specific reaction are strongly affected by the stability of reactants, intermediates, transition orbitals, and products.[44] The ability to bind the gas molecules on catalytic active centers confirms the reaction efficiency. We then investigate the adsorption of reactants CO and O_2 over Co atom(s) anchored CN.

O_2 molecule is one of the most important participants in the whole process of CO oxidation. We consider both end-on and side-on adsorption of O_2 on both Co@CN and 2Co@CN, and find that the adsorption energy via side-on is more negative (see Table 2 and Table S1); therefore, we focus on this configuration. As shown in Fig. 3(a), the O_2 molecule prefers to lie parallel to the plane of the substrate, on top of the implanted Co atom. The two nearest Co–O distances are both 1.8 Å, the O–O bond length is 1.34 Å, stretched by 0.11 Å compared with the value of free O_2(g), which indicates that the "donation–acceptance" between Co and edged N in CN that activates the reaction activity of the single Co atom. The charge transfer of 0.58$|e|$ is mainly caused by the reduction of the Co atom and accumulation of O_2 molecule (see Fig. 3(b)). Evidenced by DOS in Fig. 3(c), after adsorption, the Co-3d states are overlapped with O_2-2π^* state, the DOS peaks of O_2-5σ and O_2-1π states are downshifted, indicating that O_2 molecule accepts electrons from Co-3d orbital. The strong hybridization among them benefits the O_2 molecule to combine with Co@CN.

Table 2. The adsorption energies (eV/atom) for CO and O_2 (side-on), Bader Charge Q ($|e|$/atom), and bond length (Å) for the Co implanted CN.

System	E_a (CO)	C–O	Q	E_a (O_2)	O–O	Q
Co@CN	−1.140	1.160	0.070	−1.270	1.340	0.580
2Co@CN	−1.480	1.180	0.085	−1.430	1.500	0.700

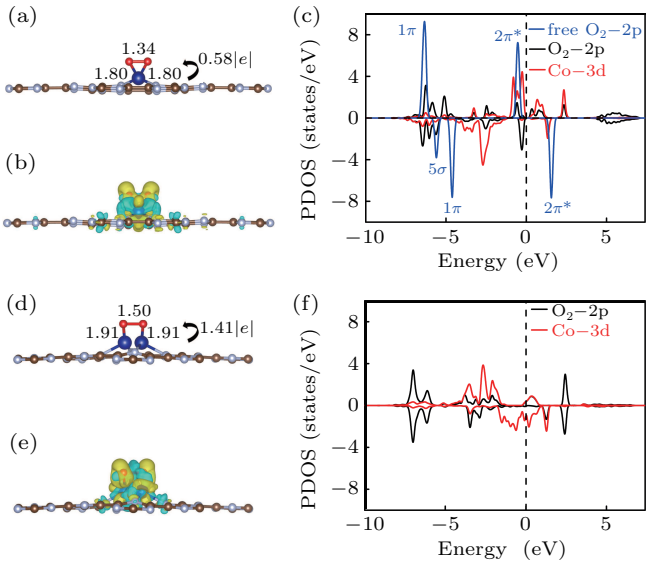


Fig. 3. The side views of the most plausible adsorption structures, the corresponding charge density difference, which iso-surface value is set to 0.003 e/Bohr^3 and the PDOS for O_2 on Co@CN (a)–(c) and 2Co@CN (d)–(f).

For 2Co@CN shown in Fig. 3(d), the O_2 molecule adsorbs over the catalyst, like a bridge connecting one Co atom to the other. The E_a of the O_2 molecule is −1.43 eV/atom, and it is relatively larger than that of the O_2 molecule on 2Cu@C_2N (−0.67 eV/atom). The bond length of O–O (1.50 Å) is longer than that of O_2 over Co@CN. Moreover, Bader charge analysis shows that each Co atom transfers 0.70$|e|$ to the O_2 molecule. After O_2 adsorbing, there are several peaks overlapping with Co-3d and O_2-2p states at the energy region of −2 eV to −5 eV, as shown in Figs. 3(c) and 3(f). For Co@CN, the O_2 molecule donates 1π and 5σ state electrons to Co-3d state, and the occupied Co-3d states feedback electrons to 2π^* state of O_2 molecule, which is evidenced by the spin-down peak near Fermi level. The ability to adsorb O_2 of both Co@CN and 2Co@CN is strong, especially the latter, with more charge (0.70$|e|$ vs. 0.58$|e|$) transferred from the substrate to O_2 molecule, the length of O–O bond is more elongated.

CO interacts strongly with the Co@CN. For the most stable configuration, the calculated E_a of CO is −1.14 eV, which is close to the value of O_2 (−1.27 eV), so CO poisoning may be avoided. As presented in Fig. 4(a), the CO molecule is not perpendicular to the Co@CN plane but is inclined. The

length of the C–Co bond is 1.82 Å. The C–O bond length increases by 0.02 Å compared to the value of free CO(g) (1.14 Å). The charge transfer is 0.07$|e|$ from the substrate to CO. From the density of states in Fig. 4(c), it can be seen that there is slight charge transfer between CO and the substrate due to the donation of CO-5σ state electrons to Co-3d state and the back-donation of Co-3d state electrons to the CO-2π^* state. For CO on 2Co@CN, the adsorbate stands above the two Co atoms and is almost perpendicular to the CN sheet (see Fig. 4(d)). The E_a of −1.48 eV/atom is closer to the value of O_2 (−1.43 eV/atom); therefore, CO poisoning will not occur. The bond lengths of C–O (1.18 Å) are also longer than that of the CO molecule on Co@CN. Moreover, Bader charge analysis shows that the adsorbed CO molecule gains 0.085 $|e|$/atom from 2Co@CN. The strong interaction between Co and CO is evidenced by the DOS in Fig. 4(f). The slight charge transferring is mainly caused by the donation of CO-4π^*, 1π, 5σ electrons to Co-3d state and back donation of Co-3d electrons to CO-2π^*. Like the adsorption of O_2, the more electrons transfer from the substrate to the CO molecule, the larger the C–O bond length.

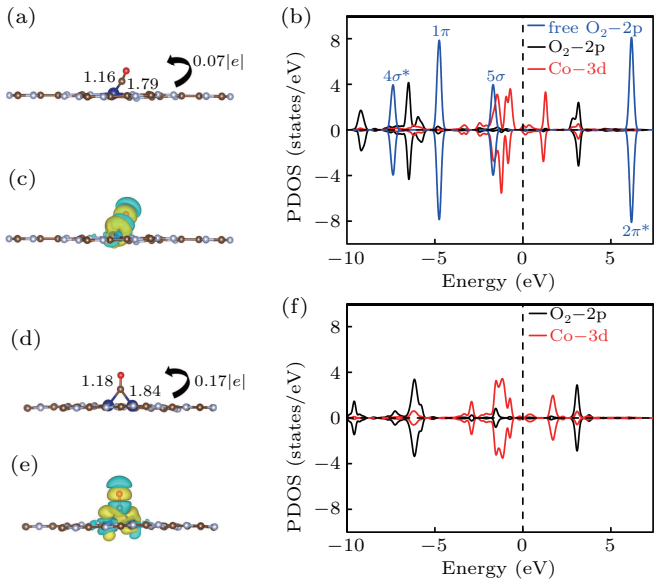


Fig. 4. The side views of the most stable adsorption structures, the corresponding charge density difference and the PDOS for CO on Co@CN (a)–(c) and 2Co@CN (d)–(f).

We also consider the final products O atomic and CO_2 adsorption on both catalysts and summarize the data in Table S1. The E_a of O atom absorbed on Co@CN and 2Co@CN is −3.94 eV and −3.14 eV, respectively. Due to the strong hybridization between the O-2p and Co-3d states, the Co–O bond length is all less than 2 Å. The bond length of the two C–O bonds, as well as the angle of O–C–O, is the same as that of free CO_2 (g). The E_a of CO_2 is −0.42 eV and −0.34 eV, respectively, both are less than 0.50 eV, indicating that CO_2 is easy to desorb.[33]

3.3. CO oxidation on Co@CN and 2Co@CN

Generally, the CO oxidation on catalysts can mainly be performed by three typical reaction mechanisms, namely Eley–Rideal (ER), Langmuir–Hinshelwood (LH), and termolecular Eley–Rideal (TER) mechanism. Considering the recycling of catalysts, we take catalysts themselves as the initial state in three mechanisms.

The ER, a mechanism of single active state participating in the reaction, is initiated by the direct reaction of gaseous CO molecules with the adsorbed O atom at the reaction centers resulting in the activation of O_2 to form a carbonate-like CO_3 intermediate or a final product of CO_2. The dissociation of O_2 is the rate-limiting step. For Co@CN, the interaction with CO is as strong as that with O_2, which can avoid CO poisoning. The configuration of physically adsorbed CO above the pre-adsorbed O_2 is selected as the initial state (IS2). As shown in Fig. S3, a chemically adsorbed atomic O and a physically adsorbed CO_2 molecule are considered as the final state (FS). In IS2, when the CO molecule approaches the activated O_2, the O–O distance increases from 1.34 Å to 1.35 Å. The insertion of CO is exothermic; the breaking of the O–O bond and the formation of the new C–O bonds need to cross a barrier of 0.73 eV. Then it forms carbonate–like CO_3 (TS1). The CO_3 in TS1 dissociates by scission of one C–O bond attached to the Co atom. The process has an energy barrier of 3.14 eV (from MS1 to TS2). As a result, there leaves a physically adsorbed CO_2 and an O atom adsorbing on the Co@CN (FS). CO_2 adsorption on Co@CN is quite weak, and entire CO oxidation is exothermic at 300 K. The ER mechanism is unfavorable due to its large reaction barriers (> 3 eV). The reaction on 2Co@CN is shown in Fig. S5. The entire reaction progress of 2Co@CN is similar to that of Co@CN, and its reaction barrier is 2.65 eV.

The LH, a mechanism of double active states ($CO + O_2$) participating in the reaction, starts with the interaction between the co-adsorbed CO and O_2 molecules for forming a peroxide-like OCOO intermediate and then the O–O bond breaks. And there leaves a physically adsorbed CO_2 together with an adsorbed atomic O like the final state of ER. As shown in Fig. S4, the co-adsorption of CO and O_2 on Co@CN is selected as the initial state (IS). Then crossing an energy barrier of 0.25 eV, CO and O_2 are parallel with end-on configurations (TS1). The CO and O_2 are activated, the O–O and C–O bonds are elongated. The peroxide-like OCOO has formed (MS1) with new O–O bond (1.63 Å). With the scission of the new O–O bond and Co–C in MS, a physically adsorbed CO_2 is formed together with an adsorbed atomic O (TS2). The reaction from MS1 to TS2 climbs the energy barriers of 0.79 eV. The entire progress is exothermic with a small reaction barrier of 1.69 eV. The reaction could process readily with the barrier of 0.8 eV or less.[44] The findings indicate that CO oxidation on Co@CN is not particularly desirable. Whereas, O_2 molecule prefers

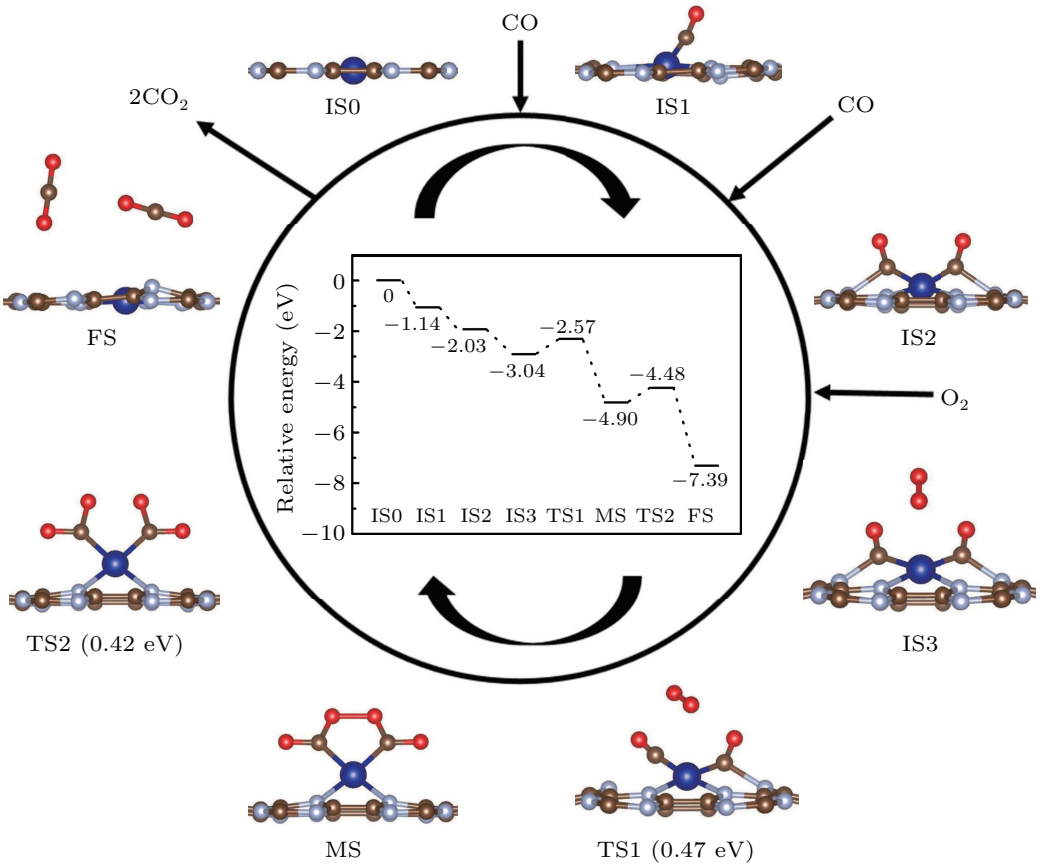


Fig. 5. Schematic energy profile corresponding to the configurations (side-view) for CO oxidation on Co@CN through TER mechanism. All energies are given with respect to the reference energies of IS0.

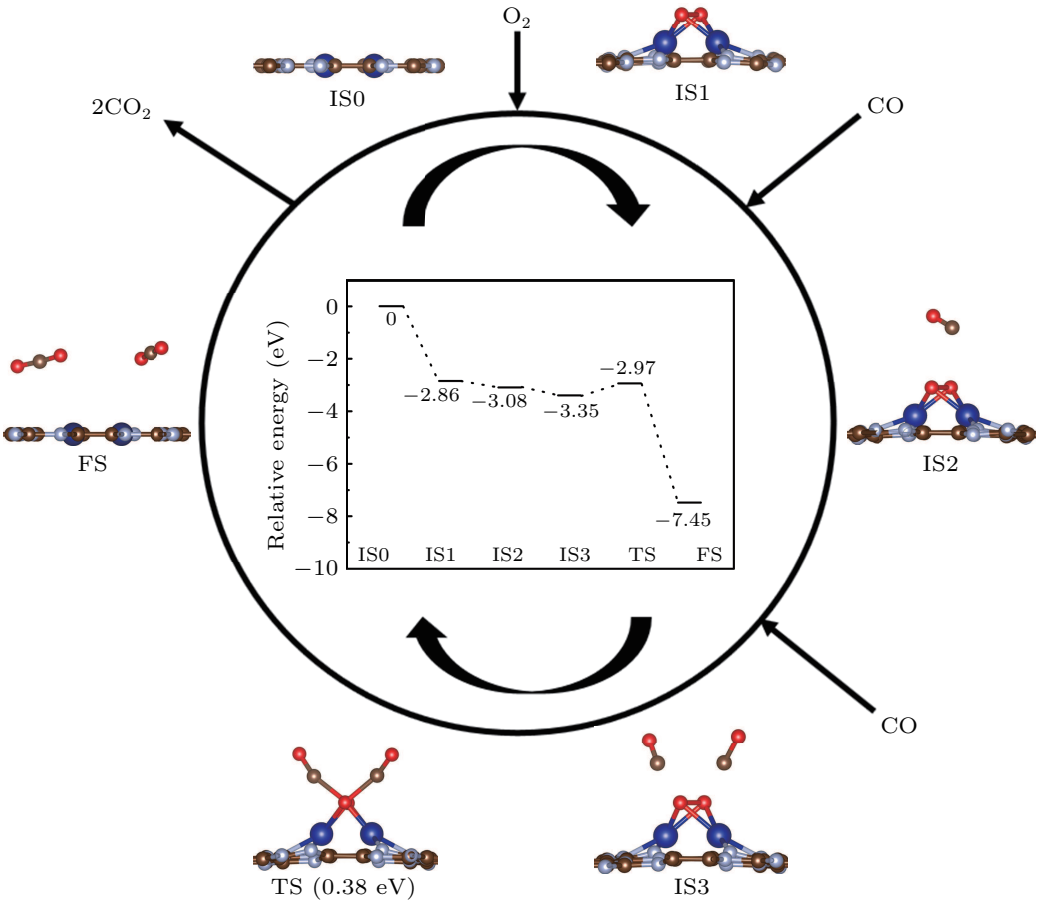


Fig. 6. Schematic energy profile corresponding to the configurations (side-view) for CO oxidation on 2Co@CN through TER mechanism.

adsorbing on 2Co@CN (IS1). With CO molecule participating in, the O–O bond stretches. Then one of the O atoms approaches to adsorbed CO molecule, and it forms OCOO (MS1). Then it gets dispersed, the corresponding reaction barrier is only 0.62 eV. We conclude that 2Co@CN is superior in terms of a minor reaction barrier. Following this, as shown in Fig. S6, the left adsorbed atomic O will react with another gaseous CO molecule (IS) and form the second physically adsorbed CO_2 (FS). For Co@CN (2Co@CN), the formation of the second CO_2 needs to pass over a reaction barrier of 0.28 eV (0.34 eV) and release the heat of 3.82 eV (2.65 eV), respectively.

Similar to the LH mechanism, the TER is a mechanism of double active states (CO + CO) participating in the reaction. Free O_2 molecule can be activated by the two co–adsorbed CO molecules to form an OCO–M–OCO intermediate. Then CO_2 molecules gradually stay away from the catalysts after the breaking of the C–Co bond. As shown in Fig. 5, two CO molecules are chemically co–adsorbed on the Co site, and one O_2 molecule approaches them from the top (IS). Then the insertion of O_2 actives the pre-adsorbed CO with the elongated O–O bond length of 1.28 Å (TS1) via adsorbing energy of 0.47 eV. Once a free O_2 is close enough, two O atoms bind to the C atoms and form an OCO–Co–OCO intermediate (MS). From MS to TS1, as the O–O bond length continues to increase, it finally breaks, and OCO–Co–OCO dissociates into two CO_2 molecules with a small reaction barrier of 0.42 eV and a huge exothermic energy of 4.35 eV (TS2). Due to the small E_a (−0.42 eV) of CO_2 on Co@CN, they should desorb spontaneously and finish the reaction cycle. The rate–limiting step for the TER mechanism is the dissociative adsorption of O_2, and the reaction energy of Co@CN is 0.42 eV. The result indicates that the CO oxidation on Co@CN through the TER mechanism is superior to Pd@CN (0.48 eV). For 2Co@CN, as shown in Fig. 6, the adsorbed O_2 molecule reacts with two CO molecules simultaneously and produces an OCO–Co–OCO intermediate.[45] The reaction barrier is 0.38 eV, a bit smaller than that of Co@CN.

4. Conclusion

We have investigated the electronic structure of one and two Co atoms implanted on CN monolayer and their catalytic role played in CO oxidation by first-principles calculations. Our results show that the large binding energy and high diffusion barrier ensure that Co atoms are steadily anchored on CN and hard to form clusters, which are beneficial for the reactions. The adsorption energies of CO and O_2 on both catalysts are comparable, and the reactants molecules can be effectively captured and activated. Via three typical reaction mechanisms, we find that CO oxidation can favorably be in progress over both catalysts, and the TER mechanism is more preferable with a fairly small rate-limiting reaction barrier.

References

[1] Luo Y, Deng Y Q, Mao W, Yang X J, Zhu K, Xu J and Han Y F 2013 *J. Phys. Chem. C* **116** 20975
[2] Qiao B, Wang A, Yang X, Allard L F, Jiang Z, Cui Y, Liu J, Li J and Zhang T 2011 *Nat. Chem.* **3** 634
[3] Lin J, Qiao B, Liu J Y, Huang Y Q, Wang A Q, Li L, Zhang W S, Allard L F, Wang X D and Zhang T 2012 *Angew. Chem. Int. Ed. Engl.* **51** 2920
[4] Li F, Li Y, Zeng X C and Chen Z 2014 *ACS Catal.* **5** 544
[5] Eiswirth M and Ertl G 1986 *Surf. Sci.* **177** 90
[6] Yamamoto T, Kasai H and Okiji A 1991 *J. Phys. Soc. Japan* **60** 982
[7] Stampfl C and Scheffler M 1997 *Phys. Rev. Lett.* **78** 1500
[8] Ying C, Hu P, Lee M H and Wang H 2008 *Surf. Sci.* **602** 1736
[9] Jiang Q G, Ao Z M, Li S and Wen Z 2014 *RSC Adv.* **4** 20290
[10] Qiao B, Wang A, Yang X, Allard L F, Jiang Z, Cui Y, Liu J, Li J and Zhang T 2011 *Nat. Chem.* **3** 634
[11] Dzuba V A, Flambaum V V, Gribakin G F and Harabati C 2012 *Phys. Rev. A* **86** 6691
[12] Balandin A A, Ghosh S, Bao W, Calizo I, Teweldebrhan D, Miao F and Lau C N 2008 *Nano Lett.* **8** 902
[13] Zhang Y, Tan Y W, Stormer H L and Kim P 2005 *Nature* **438** 201
[14] Yin Z, Li H, Li H, Jiang L, Shi Y, Sun Y, Lu G, Zhang Q, Chen X and Zhang H 2012 *ACS Nano* **6** 74
[15] Feldman Y, Wasserman E, Srolovitz D J and Tenne R 1995 *Science* **267** 222
[16] Li Y, Rao Y, Mak K F, You Y and Heinz T F 2013 *Nano Lett.* **13** 3329
[17] Liu L, Feng Y P and Shen Z X 2003 *Phys. Rev. B* **68** 104102
[18] Li Y, Ho W, Lv K, Zhu B and Lee S C 2018 *Appl. Surf. Sci.* **430** 380
[19] Zhi Y, Wang G, Bo M, He J, Zhong M, Zhao W, Li Y, Long X and Zhang W 2018 *Mater. Res. Express* **6** 035910
[20] Rao Y and Duan X 2019 *Phys. Chem. Chem. Phys.* **21** 25743
[21] Long X, Li X, Wei X and Cao J 2019 *Chem. Phys. Lett.* **725** 75
[22] Ouma C N M, Obodo K O, Braun M and Amolo G O 2018 *J. Mater. Chem. C* **6** 4015
[23] Yan H and Yang H 2011 *J. Alloys Compd.* **509** L26
[24] Liao G, Zhu D, Li L and Lan B 2014 *J. Hazard. Mater.* **280** 531
[25] Liang B, Rao Y and Duan X 2019 *RSC Adv.* **9** 38724
[26] Chen Z and Li F 2018 *Nanoscale* **10** 15696
[27] Rao Y C, Chu Z Q, Gu X and Duan X M 2019 *Comput. Mater. Sci.* **161** 53
[28] Li X, Cui P, Zhong W, Li J, Wang X, Wang Z and Jiang J 2016 *Chem. Commun.* **52** 13233
[29] Zhang G G, Zhang M W, Ye X X, Qiu X Q, Lin S and Wang X C 2014 *Adv. Mater.* **26** 805
[30] Haruta M, Tsubota S, Kobayashi T, Kageyama H, Genet M J and Delmon B 1993 *J. Catal.* **144** 175
[31] Xie X, Yong L, Liu Z Q, Haruta M and Shen W 2009 *Nature* **458** 746
[32] Tang Y, Ma D, Chen W and Dai X 2015 *Sens. Actuators B Chem.* **211** 227
[33] Lu Z, Lv P, Liang Y, Ma D, Zhang Y and Yang Z 2016 *Phys. Chem. Chem. Phys* **18** 21865
[34] Wang S, Li J, Li Q, Bai X and Wang J 2019 *Nanoscale* **12** 364
[35] Kresse G and Furthmüler J 1996 *Comput. Mater. Sci.* **6** 15
[36] Perdew J P, Burke K and Ernzerhof M 1996 *Phys. Rev. Lett.* **77** 3865
[37] Krishtal A, Vannomeslaeghe K, Olasz A, Veszprémi T, Van Alsenoy C and Geerlings P 2010 *Physics* **130** 174101
[38] Monkhorst H J and Pack J D 1976 *Phys. Rev. B* **13** 5188
[39] Liu X J, Zhou Z F, Yang L W, Li J W, Xie G F, Fu S Y and Sun C Q 2011 *J. Appl. Phys.* **109** 074319
[40] Henkelman G, Uberuaga B P and Jósson H 2000 *J. Chem. Phys.* **113** 9901
[41] Henkelman G, Arnaldsson A and Jósson H 2006 *Comput. Mater. Sci.* **36** 354
[42] Kittel C 2005 *Introduction to Solid State Physics* 8th ed. (Hoboken, NJ : Wiley)
[43] Chen D and Li F 2018 *Nanoscale* **10** 15696
[44] Deng Q, Zhao L and Gao X 2013 *Small* **9** 3506
[45] Xu G, Wang R, Yang F, Ma D, Yang Z and Lu Z 2017 *Carbon* **118** 35